RSC Advances

PAPER

View Article Online
View Journal | View Issue

Cite this: *RSC Adv.*, 2021, **11**, 9222

pH-triggered degradation and release of doxorubicin from zeolitic imidazolate framework-8 (ZIF8) decorated with polyacrylic acid†

Vy Anh Tran [ab] and Sang-Wha Lee *[a]

Zeolite imidazolate framework-8 (ZIF8) represents a class of highly porous materials with a very high surface area, large pore volume, thermal stability, and biocompatibility. In this study, ZIF8-based nanostructures demonstrated a high loading capacity for doxorubicin (62 mg Dox per g ZIF8) through the combination of π–π stacking, hydrogen bonding, and electrostatic interactions. Dox-loaded ZIF8 was subsequently decorated with polyacrylic acid (PAA) (ZIF8–Dox@PAA) that showed good dispersity, fluorescent imaging capability, and pH-responsive drug release. The stable localization and association of Dox in ZIF8@PAA were investigated by C^{13} nuclear magnetic resonance (NMR) and Fourier transform infrared spectroscopy. The NMR chemical shifts suggest the formation of hydrogen bonding interactions and π–π stacking interactions between the imidazole ring of ZIF8 and the benzene ring of Dox that can significantly improve the storage of Dox in the ZIF8 nanostructure. Additionally, the release mechanism of ZIF8–Dox@PAA was discussed based on the detachment of the PAA layer, enhanced solubility of Dox, and destruction of ZIF8 at different pH conditions. *In vitro* release test of ZIF8–Dox@PAA at pH 7.4 showed the low release rate of 24.7% even after 100 h. However, ZIF8–Dox@PAA at pH 4.0 exhibited four stages of release profiles, significantly enhanced release rate of 84.7% at the final release stage after 30 h. The release kinetics of ZIF8–Dox@PAA was analyzed by the sigmoidal Hill, exponential Weibull, and two-stage BiDoseResp models. The ZIF8–Dox@PAA nanocarrier demonstrated a promising theranostic nanoplatform equipped with fluorescent bioimaging, pH-responsive controlled drug release, and high drug loading capacity.

Received 11th December 2020
Accepted 26th January 2021

DOI: 10.1039/d0ra10423j

rsc.li/rsc-advances

1. Introduction

Zeolitic imidazolate framework 8 (ZIF8) is a class of porous materials that have been the focus of considerable interest because of their potential applications in adsorption processes, gas storage, catalysis, and drug delivery systems.[1–7] The rotational angle of the 2-methylimidazolate linker through the two nitrogen atoms leads to the flexibility of the ZIF8 framework.[8–11] The systematic variations of linker substituents can yield widely diverse framework structures that allow for the rational design of surface properties.[12–15] ZIF8 possesses extra-high porosity, chemical and thermal stability, biocompatibility, and easily controllable size and shape.[16–18]

Multifunctional ZIF8 nanomaterials have adaptability and responsiveness to various endogenous stimuli (*e.g.*, pH, enzyme, and redox gradients)[19–25] and exogenous stimuli (*e.g.*, temperature, magnetic field, and light)[26–29] and controllable drug release for disease therapy and cell imaging.[24,30] Additionally, ZIF8 nanocarriers can have various nanomedicine applications, such as targeting cancer cells with hyaluronic acid conjugates,[31] magnetic resonance and fluorescence imaging using fluorescein isothiocyanate (FITC),[19] and controlled drug release by graphene oxide.[20] Photothermal therapy, which utilizes the near-infrared laser-induced thermal ablation of cancer cells, has been widely explored and has shown significant therapeutic effects when combined with conventional chemotherapy.[32]

Although there have been many studies on the application of ZIF8 for drug transmission systems,[13] the effective absorption of a drug through various methods, such as *in situ* and multi-function steps, has been rarely investigated.[26,33] Additionally, the interaction effects between drug molecules loaded in ZIF8 nanostructures and drug release have not been well discussed in detail.[34,35] An important factor to model the release of a drug has not been well considered.[30,36–38] To the best of our knowledge, the correlation between the decomposition of ZIF8 in acid–base environments and changes in ZIF8-modified materials has not been analyzed in detail.[39,40]

In this study, we synthesized ZIF8-derived nanostructures incorporated with doxorubicin (Dox), an anticancer drug, *via*

[a]*Department of Chemical and Biological Engineering, Gachon University, 1342 Seongnamdaero, Sujeong-gu, Seongnam-si 13120, Republic of Korea. E-mail: lswha@gachon.ac.kr*

[b]*Institute of Research and Development, Duy Tan University, Danang 550000, Vietnam*

† Electronic supplementary information (ESI) available. See DOI: 10.1039/d0ra10423j

the external coating of the polyacrylic acid (PAA) layer. The localization and association of Dox in ZIF8 and its interaction with PAA were investigated by C^{13} nuclear magnetic resonance (NMR) and Fourier transform infrared (FTIR) spectroscopy. The release behavior of Dox at different pH values was investigated in terms of the detached PAA layer, enhanced solubility of Dox, and the mechanism of ZIF8 destruction under acidic conditions. The release kinetics of sigmoidal (S-shaped), exponential, and two-stage behaviors were analyzed through the combination of empirical Hill, Weibull, and BiDoseResp models. ZIF8–Dox@PAA is a promising drug delivery system with bioimaging, pH-triggered chemotherapy, and theranostic abilities.

2. Methods and experiment

2.1. Chemical materials

2-Methylimidazole (99% purity), zinc nitrate hexahydrate ($Zn(NO_3)_2 \cdot 6H_2O$, ≥99.0% purity), PAA (M_w ~450 000), and methanol (≥99.9% purity) were purchased from Sigma-Aldrich. Phosphate-buffered saline (PBS) was purchased from Bioneer (South Korea). Ethanol and water (HPLC grade) were used as received without further purification. All other chemicals were of the highest commercially available quality and used as received. The glassware was cleaned by an acidic solution of HNO_3 : HCl (3 : 1) and rinsed several times with deionized water.

2.2. Synthesis of pristine ZIF8

ZIF8 was synthesized based on previously reported procedures.[41,42] Zinc nitrate (0.60 g) and 2-methylimidazole (1.32 g) were dissolved in methanol (20.0 mL) in separate glass jars. Then, the zinc nitrate solution was rapidly poured into the 2-methylimidazole solution under constant stirring (400 rpm). The reaction was performed at room temperature (RT).

To investigate the factors that affect the structure and size of ZIF8, it was synthesized under various conditions. After mixing the two solutions, the first sample was maintained under tranquil conditions (no stirring) for 24 h. The second sample was sonicated using a sonicator (Mujigae Sonicator Model SD350H) with an average power output of 300 W and a frequency of 40 kHz. The third and fourth samples were stirred for 10 min and 30 min, respectively. Then, all mixtures were maintained under tranquil conditions for 24 h. The obtained products were collected by centrifugation at 6000 rpm for 6 min, rinsed with excess methanol, and dried in an oven at 80 °C.

2.3. Synthesis of PAA-coated ZIF8 and drug loading

Dox in methanol (2 mg mL^{-1}) of 7.5 mL was added to the 100 mg of ZIF8 NPs dispersed in 10 mL methanol. Then, the color of mixed solution became slightly red, implying the formation of Dox-loaded ZIF8. The mixture was kept at RT for 24 h and centrifuged at 5000 rpm for 5 min to obtain the Dox-loaded ZIF8. The obtained sample was washed with 10 mL of methanol several times to completely remove the Dox adsorbed outside the ZIF8 sample. The loading amount of Dox was calculated by subtracting the mass of Dox in the supernatant from the total mass of the drug in the first initial solution by UV-vis spectroscopy at 480/500 nm.[43,44]

To improve the modification ability of ZIF8 NPs, they were processed with a PAA coating layer. In water at a neutral pH, PAA is an anionic polymer; thus, many side chains of PAA lose protons and obtain a negative charge. PAA-coated ZIF8 (ZIF8@PAA) was prepared based on the electrostatic and acid–base interactions between PAA and ZIF8. Briefly, 500 mg of ZIF8–Dox NPs was dispersed in 50 mL of an aqueous solution under intensive stirring. Then, 10 mL of 10 mg mL^{-1} PAA (pH ~7.4) was added dropwise and the solution was stirred for 10 h at RT, during which PAA electrostatically attached to the surface of the ZIF8–Dox NPs. Afterward, the ZIF8–Dox@PAA NPs were separated from the PAA solution and washed in water many times to remove residual PAA.[45]

2.4. *In vitro* release test

Dox-loaded ZIF8 or Dox-loaded ZIF8 coated with PAA (ZIF8–Dox and ZIF8–Dox@PAA, respectively) was added to 10 mL of PBS (pH 7.4 and 4.0) under stirring in the dark at 37 ± 0.5 °C, which is the human physiological body temperature. To estimate the concentration of released drug, standard curves were obtained over a wide concentration range, which followed the linear behavior of the Beer–Lambert law (Fig. S1†). During an *in vitro* release test, a 6 μL aliquot was periodically sampled to monitor the release kinetics by UV-vis spectroscopy (NanoDrop; NanoDrop Technologies, Wilmington, DE, USA).

3. Results and discussion

3.1. Preparation and characterization of ZIF8-derived samples

The effect of sonication on the formation of ZIF8 was investigated under various conditions. Under sonication for 10 min, the particle size distribution became bimodal, which was supported by the scanning electron microscopy (SEM) image that showed two different populations of particles (*i.e.*, ~50 nm and ~150 nm; Fig. 1(A1)). These results support the occurrence of a sonication-induced Ostwald ripening that induces the preferential dissolution of smaller particles and recrystallization and growth into larger particles. During the sonication process, cavitation from sonic waves creates localized areas where the pressure and temperature are significantly higher than those of the surrounding medium.[46] This is followed by the diffusion of dissolved species and rapid recrystallization onto the larger particles. Because the smaller particles, with a higher surface-to-volume ratio, have low thermodynamic stability, the ripening process leads to the slow disappearance of small particles and the simultaneous growth of large particles (oriented attachment growth) to minimize the surface free energy[47,48] (Fig. 1(B1)).

The effect of stirring on the formation of ZIF8 was also investigated. The tranquil condition without stirring produced uniform and round ZIF8 (~50 nm) (Fig. 1(A2)). A narrow size distribution is only obtained without stirring during the synthetic process.[49] Under constant stirring for 10 min, ZIF8 crystals were dispersed and dodecahedral, yet uniform. The

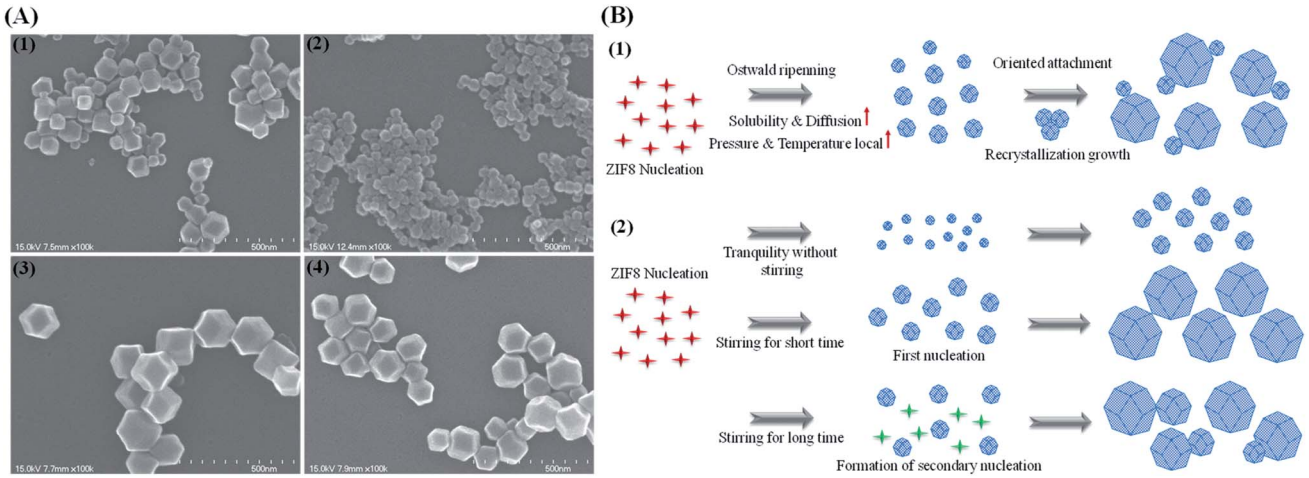

Fig. 1 (A) SEM images of ZIF8 formed at different agitation conditions: (1) sonication (power: 200 watts, frequency: 80 kHz) for 10 min, (2) tranquil without stirring, (3) constant stirring 300 rpm for 10 min, and (4) constant stirring for 40 min; (B) factors that affect the formation process and the structural morphology of ZIF8: (1) sonication effect, (2) stirring and time effect. Abbreviations: SEM, scanning electron microscopy; ZIF8, zeolite imidazolate framework-8.

average size of ZIF8 was 160 nm and the surface was smooth (Fig. 1(A1–3)). When the stirring time was increased to 40 min, ZIF8 became less uniform and decreased in size by ~10 nm (Fig. 1(A4)), probably because of secondary nucleation that causes broad size distributions.[50] After a short stirring time, the first nucleation creates the uniform and large ZIF8 particles; however, a longer stirring time induces the secondary nucleation caused by turbulence, which can form additional nucleates, resulting in the growth of small particles with the large preformed ZIF8 (Fig. 1(B1 and 2)).

3.1.1 Brunauer–Emmett–Teller (BET) and thermogravimetric (TGA) analyses. The N_2 adsorption/desorption isotherms of ZIF8 are shown in Fig. 2A. They are close to type II isotherms, belonging to the hysteresis loop of type H3.[20,51] At the initial part of the adsorption isotherm, the adsorption capacity increased sharply, which indicated an abundance of nanopores. The

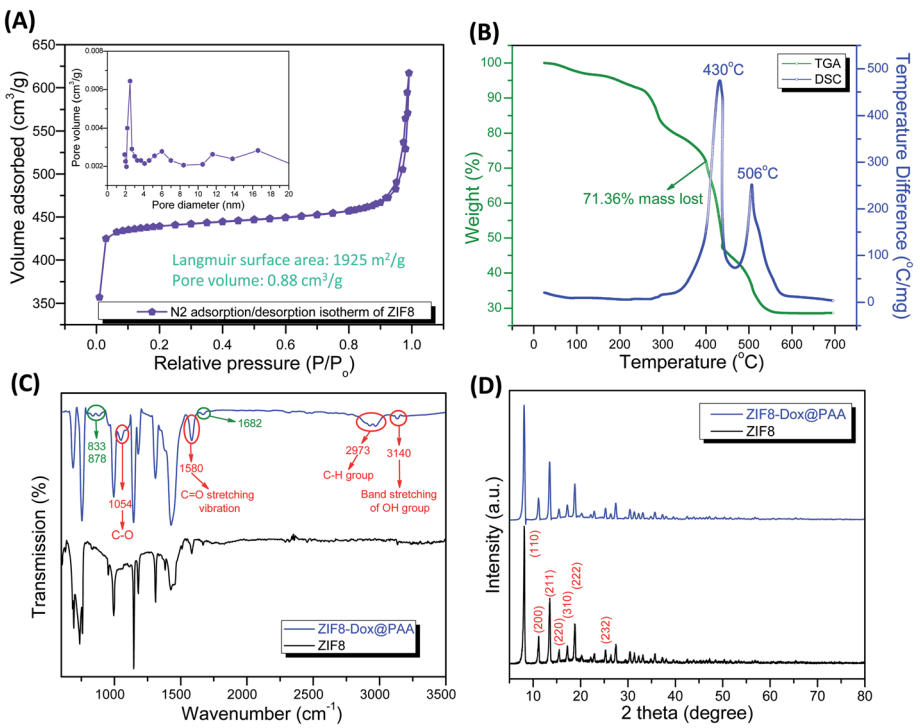

Fig. 2 (A) Nitrogen adsorption–desorption isotherm of ZIF8; (B) TGA and DSC of ZIF8 in the atmosphere; (C) FTIR spectra of ZIF8 and ZIF8–Dox@PAA; and (D) XRD spectra of ZIF8 and ZIF8–Dox@PAA. Abbreviations: DSC, differential scanning calorimetry; Dox, doxorubicin; FTIR, Fourier transform infrared; PAA, polyacrylic acid; TGA, thermogravimetric analysis; XRD, X-ray diffraction; ZIF8, zeolite imidazolate framework-8.

surface area of ZIF8, determined by BET, was 1925 $m^2 g^{-1}$ with a pore size of 2.1 nm (Fig. 2A).

TGA and differential scanning calorimetric (DSC) analyses were conducted to investigate the thermal decomposition behavior of ZIF8 at a ramping rate of 10 °C min^{-1} (Fig. 2B). The weight loss in the first stage was attributed to the evaporation of solvents, showing endothermic heat flow at 112–251 °C. In the second stage, at 252–302 °C, rapid weight loss occurred owing to the decomposition of ZIF8 in the air. In the third stage, the sharp decrease of weight loss was caused by the decomposition of organic imidazolate species into CO_2, NO_2, and H_2O effluents.[16] According to the DSC results, ZIF8 showed a high exothermic heat flow at 375–455 °C, showing the peak at 430 °C. Additionally, a low exothermic heat flow occurred at 490–550 °C. The exothermic peaks could be attributed to the cleavage of chemical bonds between zinc and 2-methylimidazole during the TGA process in air.[52] These decomposition reactions resulted in a final loss of 71.36% of the total mass.

3.1.2 FTIR and X-ray diffraction (XRD) analysis. Fig. 2C shows the FTIR spectra of the ZIF8 and ZIF8–Dox@PAA samples. The peak at 1579 cm^{-1} was attributed to the C=N stretching mode and the broad peaks at 1430 and 1305 cm^{-1} corresponded to the stretching of the entire ring. The spectral bands between 1145 and 997 cm^{-1} were ascribed to the in-plane bending of the ring and the peaks at 736 and 684 cm^{-1} were associated with aromatic sp^2 C–H bending.[16,34] After ZIF8–Dox was coated with PAA, the peak at 1682 cm^{-1} was due to the bending bands of the N–H groups. The double bands at 878 and 833 cm^{-1} were due to the primary amine NH_2 wag and N–H deformation bonds of doxorubicin, respectively.[53] The ZIF8–Dox@PAA produced new peaks at 1054 and 1580 cm^{-1}, which were attributed to C–O groups and the C=O stretching vibration of PAA. The double peak at 2973 cm^{-1} indicated the presence of C–H groups. In particular, band stretching of the OH group at 3140 cm^{-1} was observed.[54]

Fig. 2D shows the XRD patterns of the synthesized ZIF8. The diffraction peaks of ZIF8 were indexed to a cubic structure with an $I\bar{4}3m$ (217) space group (CCDC number: 602542). The peak locations and relative intensities of all diffraction peaks matched well with the simulated and published XRD patterns of ZIF8.[16,55,56] No other impurity peaks were detected, which indicated the highly crystalline structure of pure ZIF8. The diffraction peaks at 8.16°, 11.20°, 13.48°, 15.44°, 17.14°, 18.79°, 20.28°, and 25.34° corresponded to the (110), (200), (211), (220), (310), (222), (321), and (332) planes, respectively.[16,57] There was no difference in the XRD peaks of ZIF8 and ZIF8–Dox@PAA, indicating the stable structure of ZIF8 even after PAA coating.

3.2. Drug loading and *in vitro* release test of ZIF8–Dox@PAA

Herein, the multi-step synthesis of ZIF8–Dox@PAA was carried out to yield a drug delivery vehicle with an ultrahigh drug loading capacity. As summarized in Scheme 1, the drug-loaded ZIF8 was subsequently coated with a PAA layer. Dox was used as a model drug to test the pH-triggered release of ZIF8–Dox@PAA. PAA easily formed a coating layer over ZIF8 owing to electrostatic interactions between positively charged ZIF8 and negatively charged PAA. Besides, the formation of hydrogen bonding between ZIF8 and PAA improved the coverage of PAA on the substrate of ZIF8. The PAA coating layer acted as an unshakable and consolidated barrier that blocked the pore outlets of ZIF8, consequently preventing the rapid release of Dox. As PAA is biocompatible *in vitro* and *in vivo*,[58,59] PAA modification to ZIF8-based delivery systems increases the safety and biocompatibility of the vehicle for use in bio-applications.

The encapsulation of small molecules into the pores of the framework during crystal growth was dynamically coordinated to the zinc centers *via* the polar groups (*i.e.*, carboxylates and amines) or electrostatic binding between positively charged ZIF8 and negatively charged drug molecules. In general, negatively charged small molecules (*i.e.*, Dox, FITC, and camptothecin) are easily encapsulated in the positively charged ZIF8 framework, whereas neutral or positively charged molecules are poorly incorporated or weakly trapped in the porous structure of ZIF8 (*e.g.*, bisphenol A).[60]

In this study, Dox was absorbed by the ZIF8 nanostructure *via* a diffusion process. Subsequently, PAA was applied to encapsulate the ZIF8–Dox within an active surface *via* the

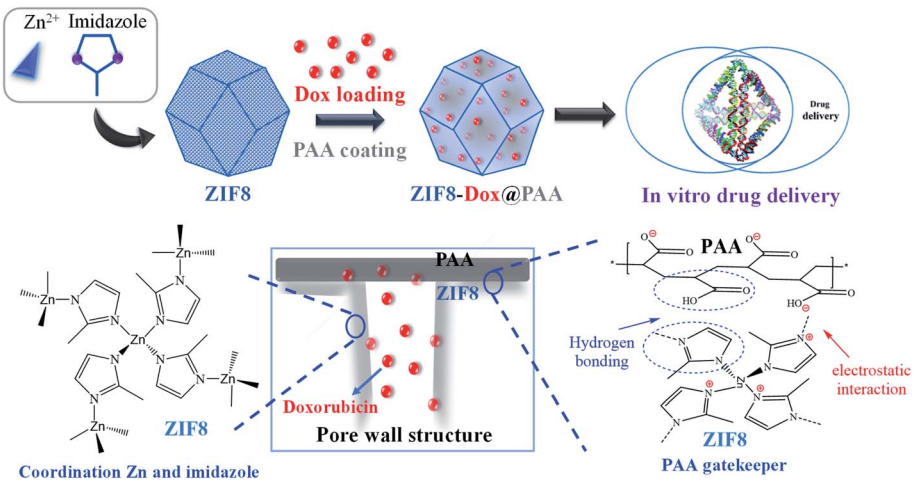

Scheme 1 Schematic illustration of the preparation of ZIF8–Dox@PAA as a vehicle for the loading and pH-controlled release of Dox and pore wall structure of ZIF8–Dox@PAA. Abbreviations: Dox, doxorubicin; PAA, polyacrylic acid; ZIF8, zeolite imidazolate framework-8.

polymerization of PAA. The synthesized ZIF8–Dox@PAA could be a potential nanocarrier for controlled drug delivery, bioimaging, and biocompatible templates (Fig. 3A). The prepared ZIF8–Dox, before and after functionalization, was explored by transmission electron microscopy (TEM). We successfully fabricated a ZIF8–Dox nanostructure, which displayed a typical hexagonal appearance with a diameter of ~150 nm (Fig. 3B). After PAA coating (Fig. 3B), the TEM image of ZIF8–Dox@PAA shows a rough surface but no significant change in the hexagonal morphology was observed. However, the surface pores of ZIF8–Dox@PAA were not observed owing to coverage by the PAA coating layer.

Fig. 3C shows the ^{13}C cross-polarization magic angle spinning NMR spectra of the ZIF8, Dox, and ZIF8–Dox samples. Compared with the ^{13}C NMR of ZIF8, that of ZIF8–Dox indicated the chemical shift of CH_3, C–N, and double carbon –C= groups. The methyl group changed from 12.94 ppm (ZIF8) to 13.95 ppm (ZIF8–Dox), which indicates the electrostatic and hydrogen bonding interactions between the ZIF8 and Dox molecules. Additionally, the chemical shift of C–N was observed from 123.27 ppm (ZIF8) to 124.35 ppm (ZIF8–Dox), along with the chemical shift of double carbon –C= from 150.41 ppm (ZIF8) to 151.42 ppm (ZIF8–Dox). These chemical shifts suggest the formation of π–π stacking interactions between the imidazole ring of ZIF8 and the benzene ring of Dox.[16,17] Based on the benzene ring structures of Dox and the imidazole of ZIF8, the intermolecular interactions are mainly attributed to π–π stacking interactions that can significantly improve the storage of Dox in the ZIF8 nanostructure. Moreover, hydrogen bonding interactions were observed for both the hydrogen of ZIF8 and the carboxylic group of Dox[16,17,61] (Fig. 3D).

An *in vitro* release test was carried out for the ZIF8–drug system at different pH conditions. The release rate of Dox-loaded ZIF8 (ZIF8–Dox) in PBS at pH 7.4 was lower than that at pH 4.0. ZIF8–Dox showed a low release rate at pH 7.4, approximately 7.0% after the first 5 h, followed by a relatively faster release of up to 22.5% after 20 h (Fig. 4A). The cumulative release of Dox reached only ~24.7%, even after 100 h. In contrast, at pH 4.0, ZIF8–Dox showed a higher release rate of Dox through four consecutive stages. At the first stage of release, 37.6% of Dox was rapidly released after only 1 h. In the second stage of release (from 1 to 10 h), Dox was slowly released and reached 45.6%. At the third stage (from 10 to 15 h), the released fraction drastically increased to 83.4%. The slight disparity in the released fraction of Dox was maintained and gradually approached an asymptotic value of 84.7% at the final stage of release after 30 h.

For ZIF8–Dox@PAA, the amount of Dox released was lower than that for ZIF8–Dox because PAA plays the role of a gatekeeper to control the transmission of Dox. During the *in vitro* release test for 10 h, only 6% Dox was released from the ZIF8–Dox@PAA at pH 7.4, followed by an asymptotic approach to the saturation value of 6.5% after 25 h. However, ZIF8–Dox@PAA at pH 4.0 exhibited four stages of release profiles that were similar to those of ZIF8–Dox, although the release rate of ZIF8–Dox@PAA was lower than that of ZIF8–Dox, probably owing to the presence of the PAA coating layer. After ZIF8–Dox detached from PAA, the Dox release profiles were significantly enhanced because of the destruction of the ZIF8 structure at pH 4.0. The

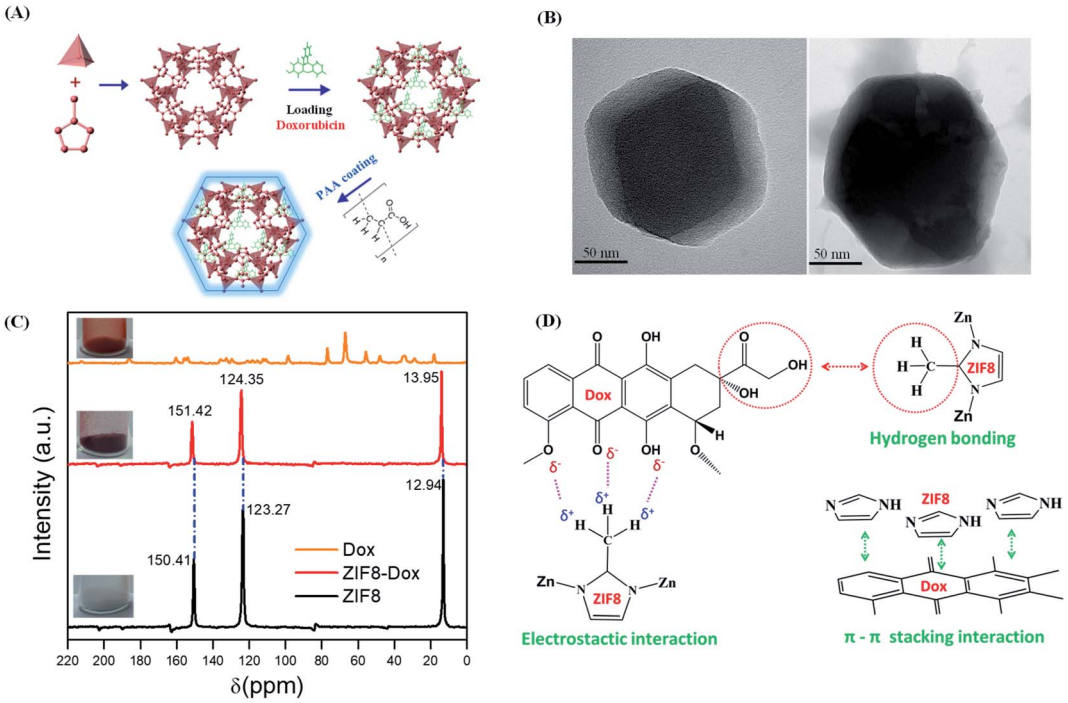

Fig. 3 (A) Illustration of trapping anticancer drug into the framework of ZIF8 by multifunctional synthesis; (B) TEM images of ZIF8–Dox (left) and multifunctional synthesis ZIF8–Dox@PAA (right); (C) NMR spectra of ZIF8, Dox, and ZIF8–Dox; (D) proposed interaction mechanisms of ZIF8 and Dox, *i.e.*, electrostatic interactions, hydrogen bonding, and π–π stacking interactions. Abbreviations: Dox, doxorubicin; PAA, polyacrylic acid; TEM, transmission electron microscopy; ZIF8, zeolite imidazolate framework-8.

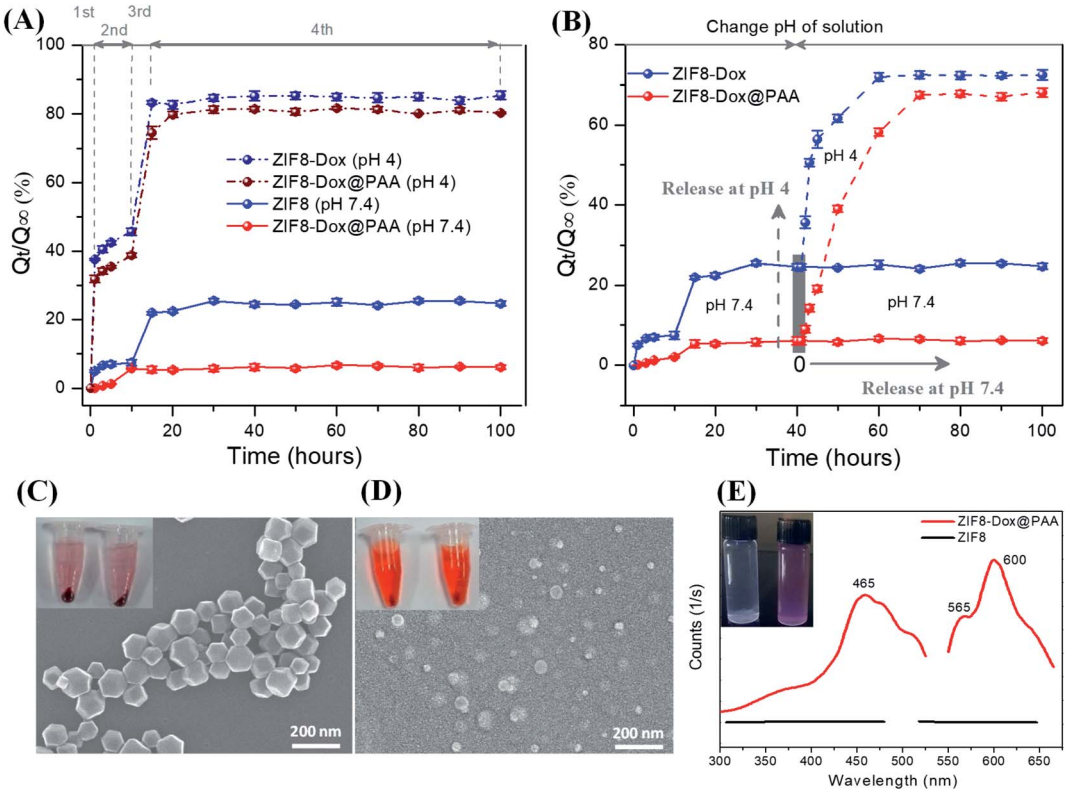

Fig. 4 (A) Release profiles of Dox from ZIF8–Dox and ZIF8–Dox@PAA in PBS under pH 7.4 and pH 4.0 at 37 °C; (B) release profiles of Dox at two different pH conditions, change in pH after the first 40 h; SEM images of ZIF8–Dox@PAA before (C) and after (D) degradation after first 1 h under pH 4.0 (the inset image of release Dox solution and aggregation of nanoparticles from ZIF8–Dox@PAA after centrifugation after first 1 h under pH 7.4 (C) and pH 4.0 (D); (E) fluorescent images and photoluminescence of synthesized ZIF8 and ZIF8–Dox@PAA samples. Abbreviations: Dox, doxorubicin; PAA, polyacrylic acid; PBS, phosphate-buffered saline; SEM, scanning electron microscopy; ZIF8, zeolite imidazolate framework-8.

released fraction of Dox showed a rapid increase to 31.8% for the first 1 h, followed by a relatively slower increase to 38.8% after 10 h during the second stage of release. In the third stage, the released fraction continuously increased to 74.5% at 15 h, and slowly approached an asymptotic value of 81.3% after 30 h (at the final stage) (Fig. 4A).

3.2.1 pH-responsive drug delivery. To evaluate the release profiles of Dox from ZIF8–Dox and ZIF8–Dox@PAA, two stages of the drug release profile were investigated by changing the solution pH after the first 40 h release (Fig. 4B). To simulate drug-loaded ZIF8 passing through a healthy cell environment, the first stage of Dox release from a ZIF8–based delivery system (ZIF8–Dox and ZIF8–Dox@PAA) was carried out at pH 7.4. As expected, the release rate of ZIF8–Dox was higher than that of ZIF8–Dox@PAA. During the first 3 h, only 1.2% Dox was released from ZIF8–Dox@PAA but the released fraction from ZIF8–Dox was 6.6%. At 30 h, the released fraction gradually reached 5.7% (ZIF8–Dox@PAA) and 25.5% (ZIF8–Dox). A further increase in the release time did not increase the released fraction, *i.e.*, 6.1% of Dox release (with PAA) and 25% of Dox release (without PAA) at 40 h. These results indicate that ZIF8–Dox@PAA exhibits a more stable and sustained release in the neutral environment than the PAA-free analog.

When the pH solution was changed from 7.4 to 4.0 (cancer cell environment), the ZIF8–Dox exhibited a rapid increase in the released fraction to 50.6% and 56.4% after 3 h and 5 h, respectively. The released fractions again increased to 61.6% and 71.9% after 10 and 20 h, respectively. The released fraction of Dox finally approached an asymptotic value of 72.5% after the final release time of 60 h. Under a decreasing pH solution, ZIF8–Dox@PAA exhibited the fastest release rate and remarkably sensitive release at pH 4.0. The disparity in the release rate was attributed to the combination of three effects: detachment of the PAA layer, enhanced solubility of Dox in the acidic environment, and destruction of the ZIF8 nanostructure. At pH 4.0, the released fraction of 6.1% increased three (19.1%) and six-fold (39.0%) after 5 h and 10 h, respectively. The disparity of released fractions continuously increased to 58.2% after 20 h. Then, the released fraction approached a saturation value of 67.5% after 30 h. When ZIF8–Dox was immersed in PBS at pH 4.0, the spherical shape of the NPs changed into irregular shapes because of the decomposition of the ZIF8 framework (Fig. 4C and D). After ZIF8 was destroyed at the final stage, Zn^{2+} ions and imidazolates originated from ZIF8 nanostructure showed the biocompatibility and no significant influence on cell viability, even up to concentrations of 50 μg mL^{-1}, as reported by previous

studies.[62–64] The sediment amounts of ZIF8–Dox@PAA after centrifugation at the bottom of the plastic tube at pH 4.0 was negligible compared with the large amounts of the sample at pH 7.4. Additionally, the ZIF8–Dox@PAA solution at pH 4.0 was dark red, which indicated that large amounts of Dox were present in the PBS solution after destructive release. Furthermore, at pH 7.4, the ZIF8-Dox@PAA solution was light red because of the small amount of Dox release.

Fig. 4E presents the photoluminescence (PL) and fluorescent images of pristine ZIF8 and ZIF8–Dox at both excitation (λ_{ex}) and emission (λ_{em}) wavelengths. The distinguishable concentration of ZIF-8-Dox@PAA by PL was 0.82 μg mL^{-1}. From this result, the concentration of detectable doxorubicin was estimated as ~0.052 μg mL^{-1}. This value is consistent with the previous studies for the detection of doxorubicin by PL.[65] This concentration is suitable to apply for bioimaging from confocal microscopic fluorescence images.[66] From the slight milk-white of the pristine ZIF8 in PBS, the solution changed to purple after Dox was loaded into ZIF8. Pristine ZIF8 showed no PL spectra, whereas Dox-loaded ZIF8 revealed the distinct PL spectra of Dox molecules. Dox-loaded ZIF8 exhibited significantly higher fluorescence intensities at 30 μg mL^{-1} than pristine ZIF8. These spectra present two emission peaks of Dox at 565 nm and 600 nm under broadband excitation at 465 nm. Thus, the PL spectra confirmed the successful trapping of Dox in the ZIF8, which indicates that this fluorescence property could be used to monitor cellular uptake and drug delivery behaviors.[19] UV-vis and PL spectra of as-prepared samples (ZIF8, ZIF8–Dox@PAA, and Doxorubicin) to show the difference of ZIF8 before and after loading Dox and coating with PAA were presented in Fig. S3.†

3.3. Analysis of pH-triggered release kinetics of ZIF-derived nanocarriers

The release kinetics of ZIF8–Dox@PAA at pH 7.4 can be analyzed using the empirical Hill equation:

$$\frac{Q_t}{Q_\infty} = \frac{Q_{\max} t^\gamma}{Q_{1/2} + t^\gamma} \quad (1)$$

where Q_{max} is the maximum amount of drug release, $Q_{1/2}$ is the time required for 50% drug release, and γ is a sigmoidicity factor. The Hill equation can suitably describe release profiles with sigmoidal behavior.

The release kinetics of Dox from ZIF8–Dox at pH 7.4 can also be predicted by an exponential equation based on the Weibull equation, the Weibull model:

$$\frac{Q_t}{Q_\infty} = A\left(1 - \exp^{-k_w (t-T)^{0.5}}\right) \quad (2)$$

where Q_t/Q_∞ is the amount of drug released as a function of time t, A is the total amount of drug released, T accounts for the lag time measured as a result of the release process, and the parameter constant k_w describes an exponential profile.

Additionally, the release kinetics of Dox from the pure ZIF8–drug system at pH 4.0 can be predicted by a sigmoidal equation based on the BiDoseResp function, the BiDoseResp model:

$$\frac{Q_t}{Q_\infty} = \frac{Q_1}{Q_\infty} + \left(\frac{Q_2}{Q_\infty} - \frac{Q_1}{Q_\infty}\right)\left[\frac{A}{1 + 10^{\log((t_1 - t)^{0.5}) h_1}} + \frac{1 - A}{1 + 10^{\log((t_2 - t)^{0.5}) h_2}}\right] \quad (3)$$

where Q_t/Q_∞ is the released fraction of the drug at time t; Q_1/Q_∞ and Q_2/Q_∞ are the released percentage of Dox at the start and finish processes, respectively; h_1 and h_2 are the Hill slope corresponding to the two-stage release; t, t_1, and t_2 are the release times of processing and the first and second stages, respectively; and A is the relaxation rate constant.

Fig. 5A shows the model fit of the Dox release profiles at pH 7.4. The release kinetics of ZIF8–Dox can be interpreted as first Fickian diffusion followed by exponential release at the second stage that can be fitted by the Weibull model. After the first released fraction of 7.4%, ZIF8–Dox showed the second release of Dox, which was a burst release to a saturation value of 25.5%. Using the Weibull model, the lag time (T) and exponential profile (k_w) of the second release process are fitted as 3.0 and 2.2, respectively (Table S1†). However, Dox release from ZIF8–Dox@PAA follows the sigmoidal behavior fitted by the Hill equation, in which the sigmoidicity factor was 5.2 (Table S1†). At the first stage of release, ZIF8–Dox@PAA showed a very low released fraction of 1.2%, caused by the restriction of Dox diffusion by the PAA layer. The fast release stage occurred shortly after, to the saturation value (5.7%). This release profile occurred owing to the mechanical lag processing of the PAA coating and the diffusion of Dox caused by its good solubility in water. In summary, at pH 7.4, the release kinetics of ZIF8–Dox–PAA can be controlled by the PAA layer because of restricted diffusion by the PAA barrier.

The release kinetics of both samples followed the BiDoseResp model (Fig. 5B). After the initial release (stage I), an accelerated burst release occurred (stage II) as drug molecules situated on the outer surface of the ZIF8 framework migrated into the release medium owing to the degradation of the outer layers at pH 4.0 (Fig. 5C). At stage III, both ZIF8–Dox and ZIF8–Dox@PAA showed drug release stagnation. This slow stage of release occurred owing to the gradual degradation of the ZIF8 framework after all drug molecules located in the outer framework had been released. Additionally, the outer layer of the ZIF8 fragments prevented the release of inner Dox. At the final stage, IV, ZIF8–Dox exhibited continuous drug release but the release rate was slightly decreased, *i.e.*, the curve slope of stage IV ($h_2 = 3.20$) was higher than that of stage II ($h_1 = 2.50$). ZIF8–Dox@PAA exhibited strong Dox release profiles at this stage, which corresponded to the reduced slopes from 3.20 (h_1, stage II) to 2.0 (h_2, stage IV) (Table S2†), owing to the hindered release of Dox by the PAA layers in stage II. However, the ZIF8 structure was broken at stage IV, which, consequently, led to rapid Dox release, approaching the asymptotic saturation state. In summary, both ZIF8–Dox and ZIF8–Dox@PAA show high degrees of deterioration at pH 4.0. Therefore, Dox more easily diffuses out and is almost completely released (stage V).[67]

3.3.1 Release mechanism. At an acidic pH, dissociation occurs by the detachment of the coordination between Zn metal ions and organic imidazole ligands (Fig. 5D).[68] This leads to the

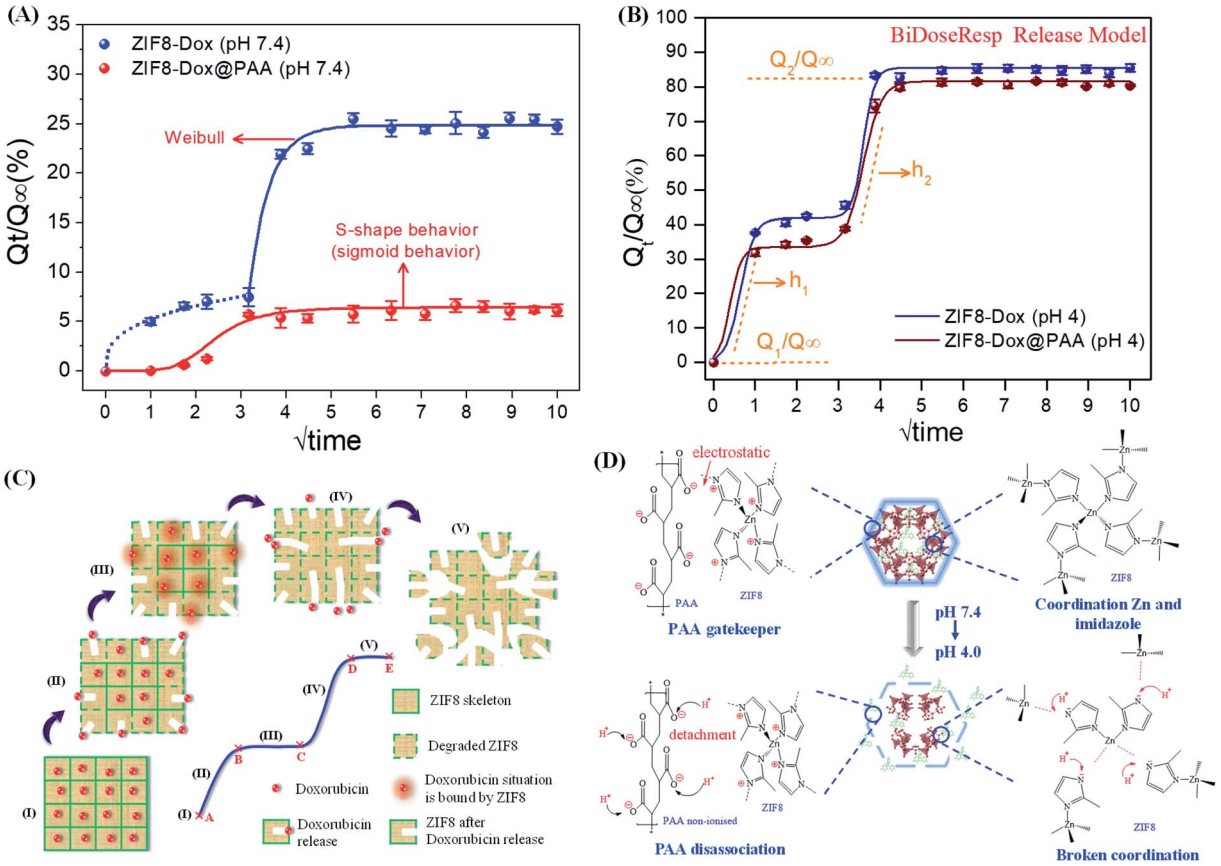

Fig. 5 Model fits of Dox release profiles from ZIF8–Dox and ZIF8–Dox@PAA in PBS at 37 °C (A) at pH 7.4 and (B) at pH 4; (C) illustration of release stages for ZIF8–Dox at pH 4.0; and (D) release processing mechanism of Dox from ZIF8–Dox@PAA with decreasing pH from 7.4 to 4.0 in PBS solution. Abbreviations: Dox, doxorubicin; PAA, polyacrylic acid; PBS, phosphate-buffered saline; ZIF8, zeolite imidazolate framework-8.

destruction of the ZIF8 structure and increases Dox release from ZIF8–Dox and ZIF8–Dox@PAA. Thus, the ZIF8@PAA system, with pH-dependent drug release, is promising for use as a drug carrier and to target cancerous tissues, as the extracellular pH of tumors is lower than that of normal tissues and the microenvironments of tumors are acidic. Another factor that affects the release process is the solubility of Dox under different pH conditions. The model drug Dox hydrochloride, a poorly water-soluble anticancer drug, was loaded into the pores of ZIF8/ZIF8@PAA to assess the drug release behavior. At a low pH, Dox solubility is improved in water; thus, the release of Dox from the ZIF8/ZIF8@PAA structure was enhanced.[69]

A drug nanocarrier with pH-triggered release is suitable to target cancer cells. The human body naturally exhibits different pH values, such as in the stomach (pH ~3.0) and the colon (pH ~7.5).[70,71] PAA was employed as the gatekeeper to control cargo transport. At a neutral pH, PAA is an anionic polymer, *i.e.*, many of the side chains of PAA lose their protons and acquire a negative charge (−17.12 mV) owing to a COO^- group, which causes PAA to form a coating layer with a positive ZIF8 surface (+37.3 mV) through electrostatic interactions. Therefore, in a neutral environment, the PAA layer became unshakable and formed a dense barrier on the pores of ZIF8–Dox@PAA, thereby preventing the release of Dox by closing the pores. In a low pH environment (at pH 4), PAA gains protons and becomes non-ionized. This leads to a change in the surface charge of the PAA layer, which weakens the electrostatic interaction with the positive ZIF8 surface. Thus, Dox is easily released from the ZIF8–Dox@PAA because the pore outlets are opened by the detachability of the PAA layer (Fig. 5D). Surface modification is a commonly used approach to improve the biocompatibility of nanomaterials for safe biomedical application. Owing to the low protein adsorption in serum and weak interaction with macrophages, PAA is biocompatible *in vitro* and *in vivo*.[72] Thus, PAA modification represents a safe method to improve the biocompatibility of ZIF8 for future biomedical use.[73]

The relevant studies were listed and compared to highlight the superiority of our research work, which was summarized in Table 1. In this work, we demonstrated the high loading capacity of ZIF8 for doxorubicin through the combination of π–π stacking, hydrogen bonding, and electrostatic interactions. The stable localization and association of Dox in ZIF8@PAA were confirmed by ^{13}C nuclear magnetic resonance and Fourier transform infrared spectroscopy. Besides, the release mechanism of ZIF8–Dox@PAA was discussed based on the detachment of the PAA layer, enhanced solubility of Dox, and

Table 1 Summary of studies on the drug delivery by metal–organic framework (MOF)

MOF	Kind drug of store	Interaction mechanism Drug-MOF	Model of release kinetic	Amount drug loading (mg drug per g carrier)	Effects to drug release	Modified agent	Ref.
ZIF8	6-Mercaptopurine	Not	Not	Not	pH condition	Not	34
ZIF8	Benznidazole	Hydrogen bonding *via* FTIR spectra	Not	Not	pH condition	Not	74
MIL-53 (Al); MIL-101 (Cr)	Thymol	The assumption of hydrogen and π–π bonding interaction	Not	9.3 10.2	pH condition	Not	75
MIL-88B (Fe)	Ibuprofen	Hydrogen-bonding and weak van der Waals interactions FTIR spectra	Hill equation	Not	Not	Not	76
ZIF8	Doxorubicin	Not	Not	15.7	Solubility of doxorubicin at low pH	Folic acid	77
ZIF8	5-Fluorouracil	Not	Not	30.0	pH condition	Polyaniline	78
ZIF8	Curcumin	π–π* transitions *via* UV-vis and NMR proton	Not	Not	Acidic condition	Not	24
MIL-100	Docetaxel	Not	Not	Not	pH condition	Not	79
MIL-100	Isoniazid	Not	Freundlich and Langmuir models	Not	Not	Not	80
ZIF8	Doxorubicin	π–π stacking interactions, hydrogen bonding, and electrostatic interactions *via* ^{13}C CP/MAS NMR; FTIR spectra, photoluminescence	Sigmoidal behavior (S-shaped behavior), BiDoseResp, and Weibull models	62.0	pH condition, solubility of doxorubicin	Poly acrylic acid	This work

destruction of ZIF8 at neutral and acidic pH conditions. Especially, the release kinetics of ZIF8–Dox@PAA was analyzed using three different models such as sigmoidal Hill, exponential Weibull, and two-stage BiDoseResp models. The ZIF8–Dox@PAA nanocarrier demonstrated a promising theranostic nanoplatform equipped with fluorescent bioimaging, pH-responsive controlled drug release, and high drug loading capacity.

4. Conclusions

ZIF8 is a class of porous materials that exhibit a high surface area, well-defined pore size, and hybrid organic–inorganic nature. The Dox drug was first loaded into the ZIF8 structure and Dox-loaded ZIF8 (ZIF8–Dox) was subsequently coated with PAA (ZIF8–Dox@PAA). The stable localization and association of Dox in ZIF8 and its interaction with PAA were investigated by C^{13} NMR and FTIR spectra. The high loading of Dox by the ZIF8 nanostructure was possible through its extra-high porosity, surface area, and physical–chemical bonds (such as π–π stacking interactions, hydrogen bonding, electrostatic interaction, and pore/size-selective adsorption). The release of Dox was carried out at different pH conditions. The influencing factors on the release were determined as the detachment of the PAA layer, enhanced solubility of Dox, and destruction of the ZIF8 structure at acidic pH condition. The kinetic release profiles of Dox from ZIF8–Dox and ZIF8–Dox@PAA were analyzed through the combination of diffusion models, such as sigmoidal behavior (S-shaped behavior), BiDoseResp, and Weibull models. The ZIF8–Dox@PAA demonstrated high drug loading capacity, fluorescent bioimaging, and pH-triggered drug release, suggesting as a good candidate for a theranostic nanoplatform.

Conflicts of interest

There are no conflicts to declare.

Acknowledgements

This study was supported by the Korea Institute of Energy Technology Evaluation and Planning (KETEP) and the Ministry of Trade, Industry, and Energy (MOTIE) of the Republic of Korea [Grant No. 20194030202440]; and a Korea Basic Institute (National Research Facilities and Equipment Center) grant funded by the Ministry of Education [Grant No. 2019R1A6C1010016].

References

1 X. Xu, H. Wang, J. Liu and H. Yan, The applications of zeolitic imidazolate framework-8 in electrical energy storage devices: a review, *J. Mater. Sci.: Mater. Electron.*, 2017, **28**(11), 7532–7543.

2 S. Lee, J. Kim, J. Kim and D. Lee, Zeolitic Imidazolate Framework Membrane with Marked Thermochemical Stability for High-Temperature Catalytic Processes, *Chem. Mater.*, 2018, **30**(2), 447–455.

3 V. T. Le, V. D. Doan, V. A. Tran, H. S. Le, D. L. Tran, T. M. Pham, T. H. Tran and H. T. Nguyen, Cu/Fe3O4@carboxylate-rich carbon composite: One-pot synthesis, characterization, adsorption and photo-Fenton catalytic activities, *Mater. Res. Bull.*, 2020, **129**, 110913.

4 A. N. Kadam, D. P. Bhopate, V. V. Kondalkar, S. M. Majhi, C. D. Bathula, A.-V. Tran and S.-W. Lee, Facile synthesis of Ag-ZnO core–shell nanostructures with enhanced photocatalytic activity, *J. Ind. Eng. Chem.*, 2018, **61**, 78–86.

5 H.-T. T. Nguyen, V.-P. Dinh, Q.-A. N. Phan, V. A. Tran, V.-D. Doan, T. Lee and T. D. Nguyen, Bimetallic Al/Fe Metal-Organic Framework for highly efficient photo-Fenton degradation of rhodamine B under visible light irradiation, *Mater. Lett.*, 2020, **279**, 128482.

6 H. H. Do, Q. V. Le, M. A. Tekalgne, A. V. Tran, T. H. Lee, S. H. Hong, S. M. Han, S. H. Ahn, Y. J. Kim, H. W. Jang and S. Y. Kim, Metal–organic framework-derived MoSx composites as efficient electrocatalysts for hydrogen evolution reaction, *J. Alloys Compd.*, 2021, **852**, 156952.

7 M. U. Dao, H. S. Le, H. Y. Hoang, A. V. Tran, V. D. Doan, T. T. N. Le, A. S. Sirotkin and V. T. Le, Natural core-shell structure activated carbon beads derived from Litsea glutinosa seeds for removal of methylene blue: Facile preparation, characterization, and adsorption properties, *Environ. Res.*, 2020, 110481.

8 S. A. Moggach, T. D. Bennett and A. K. Cheetham, The Effect of Pressure on ZIF-8: Increasing Pore Size with Pressure and the Formation of a High-Pressure Phase at 1.47 GPa, *Angew. Chem.*, 2009, **121**(38), 7221–7223.

9 H. Tanaka, S. Ohsaki, S. Hiraide, D. Yamamoto, S. Watanabe and M. T. Miyahara, Adsorption-Induced Structural Transition of ZIF-8: A Combined Experimental and Simulation Study, *J. Phys. Chem. C*, 2014, **118**(16), 8445–8454.

10 V. Anh Tran, T. Khoa Phung, V. Thuan Le, T. Ky Vo, T. Tai Nguyen, T. Anh Nga Nguyen, D. Quoc Viet, V. Quang Hieu and T.-T. Thi Vo, Solar-light-driven photocatalytic degradation of methyl orange dye over Co3O4-ZnO nanoparticles, *Mater. Lett.*, 2021, **284**, 128902.

11 V. A. Tran, T. P. Nguyen, V. T. Le, I. T. Kim, S.-W. Lee and C. T. Nguyen, Excellent photocatalytic activity of ternary Ag@WO3@rGO nanocomposites under solar simulation irradiation, *J. Sci.: Adv. Mater. Devices*, 2021, **6**, 108–117.

12 B. Wang, A. P. Côté, H. Furukawa, M. O'Keeffe and O. M. Yaghi, Colossal cages in zeolitic imidazolate frameworks as selective carbon dioxide reservoirs, *Nature*, 2008, **453**, 207.

13 S. Feng, X. Zhang, D. Shi and Z. Wang, Zeolitic imidazolate framework-8 (ZIF-8) for drug delivery: A critical review, *Front. Chem. Sci. Eng.*, 2020, 8.

14 V.-H. Nguyen, T.-T. Thi Vo, H. Huu Do, V. Thuan Le, T. Duy Nguyen, T. Ky Vo, B.-S. Nguyen, T. Tai Nguyen, T. Khoa Phung and V. Anh Tran, Ag@ZnO Porous Nanoparticle Wrapped by rGO for the Effective CO2 Electrochemical Reduction, *Chem. Eng. Sci.*, 2020, 116381.

15 H. H. Do, Q. V. Le, T. V. Nguyen, K. A. Huynh, M. A. Tekalgne, V. A. Tran, T. H. Lee, J. H. Cho, M. Shokouhimehr, S. H. Ahn, H. W. Jang and S. Y. Kim, Synthesis of MoSx/Ni-metal–organic framework-74 composites as efficient electrocatalysts for hydrogen evolution reactions, *Int. J. Energy Res.*, 2021, 852.

16 V. A. Tran, A. N. Kadam and S.-W. Lee, Adsorption-assisted photocatalytic degradation of methyl orange dye by zeolite-imidazole-framework-derived nanoparticles, *J. Alloys Compd.*, 2020, **835**, 155414.

17 V. Anh Tran, K. B. Vu, T.-T. Thi Vo, V. Thuan Le, H. H. Do, L. G. Bach and S.-W. Lee, Experimental and computational investigation on interaction mechanism of Rhodamine B adsorption and photodegradation by zeolite imidazole frameworks-8, *Appl. Surf. Sci.*, 2021, **538**, 148065.

18 V. T. Le, V. A. Tran, D. L. Tran, T. L. H. Nguyen and V.-D. Doan, Fabrication of Fe3O4/CuO@C composite from MOF-based materials as an efficient and magnetically separable photocatalyst for degradation of ciprofloxacin antibiotic, *Chemosphere*, 2021, **270**, 129417.

19 A. V. Tran, K. Shim, T. T. Vo Thi, J. K. Kook, S. S. A. An and S. W. Lee, Targeted and controlled drug delivery by multifunctional mesoporous silica nanoparticles with internal fluorescent conjugates and external polydopamine and graphene oxide layers, *Acta Biomater.*, 2018, 397–413.

20 V. A. Tran and S. W. Lee, A prominent anchoring effect on the kinetic control of drug release from mesoporous silica nanoparticles (MSNs), *J. Colloid Interface Sci.*, 2018, **510**, 345–356.

21 J. K. Kook, D. Koh, A. V. Tran and S. Lee, *Boronic acid-functionalized magnetic nanocomposites for an efficient extraction of dopamine molecules and their detection using fluorescent polydopamine*, 2017 22nd Microoptics Conference (MOC), 2017, pp. 362–363.

22 V. V. Tran VA, K. Shim and S. W. Lee, An SSA, Multimodal Mesoporous Silica Nanocarriers for Dual Stimuli-Responsive Drug Release and Excellent Photothermal Ablation of Cancer Cells, *Int. J. Nanomed.*, 2020, **15**, 7667–7685.

23 C. Y. Sun, C. Qin, X. L. Wang, G. S. Yang, K. Z. Shao, Y. Q. Lan, Z. M. Su, P. Huang, C. G. Wang and E. B. Wang, Zeolitic Imidazolate framework-8 as efficient pH-sensitive drug delivery vehicle, *Dalton Trans.*, 2012, **41**(23), 6906–6909.

24 A. Tiwari, A. Singh, N. Garg and J. K. Randhawa, Curcumin encapsulated zeolitic imidazolate frameworks as stimuli responsive drug delivery system and their interaction with biomimetic environment, *Sci. Rep.*, 2017, **7**(1), 12598.

25 M. Wu, H. Ye, F. Zhao and B. Zeng, High-Quality Metal–Organic Framework ZIF-8 Membrane Supported on

Electrodeposited ZnO/2-methylimidazole Nanocomposite: Efficient Adsorbent for the Enrichment of Acidic Drugs, *Sci. Rep.*, 2017, **7**, 39778.

26 C. Adhikari, A. Das and A. Chakraborty, Zeolitic Imidazole Framework (ZIF) Nanospheres for Easy Encapsulation and Controlled Release of an Anticancer Drug Doxorubicin under Different External Stimuli: A Way toward Smart Drug Delivery System, *Mol. Pharm.*, 2015, **12**(9), 3158–3166.

27 Y. Li, J. Jin, D. Wang, J. Lv, K. Hou, Y. Liu, C. Chen and Z. Tang, Coordination-responsive drug release inside gold nanorod@metal–organic framework core–shell nanostructures for near-infrared-induced synergistic chemo-photothermal therapy, *Nano Res.*, 2018, **11**(6), 3294–3305.

28 M. A. Chowdhury, The applications of metal–organic-frameworks in controlled release of drugs, *Rev. J. Chem.*, 2017, **7**(1), 1–22.

29 E.-B. Lim, T. A. Vy and S.-W. Lee, Comparative release kinetics of small drugs (ibuprofen and acetaminophen) from multifunctional mesoporous silica nanoparticles, *J. Mater. Chem. B*, 2020, **8**(10), 2096–2106.

30 N. H. T. T. Vy Anh Tran, Long Giang Bach, Trinh Duy Nguyen, Thi Thuong Nguyen, Tan Tai Nguyen, Thi Anh Nga Nguyen, The Ky Vo, Thu-Thao Thi Vo, Van Thuan Le, Facile Synthesis of Propranolol and Novel Derivatives, *J. Chem.*, 2020, **2020**(10), 10.

31 Q. Zhao, S. Wang, Y. Yang, X. Li, D. Di, C. Zhang, T. Jiang and S. Wang, Hyaluronic acid and carbon dots-gated hollow mesoporous silica for redox and enzyme-triggered targeted drug delivery and bioimaging, *Mater. Sci. Eng. C*, 2017, **78**, 475–484.

32 D. Wang, Z. Guo, J. Zhou, J. Chen, G. Zhao, R. Chen, M. He, Z. Liu, H. Wang and Q. Chen, Novel Mn3 [Co(CN)6] 2@SiO2@Ag Core-Shell Nanocube: Enhanced Two-Photon Fluorescence and Magnetic Resonance Dual-Modal Imaging-Guided Photothermal and Chemo-therapy, *Small*, 2015, **11**(44), 5956–5967.

33 J. Zhuang, C. H. Kuo, L. Y. Chou, D. Y. Liu, E. Weerapana and C. K. Tsung, Optimized metal–organic-framework nanospheres for drug delivery: evaluation of small-molecule encapsulation, *ACS Nano*, 2014, **8**(3), 2812–2819.

34 H. Kaur, G. C. Mohanta, V. Gupta, D. Kukkar and S. Tyagi, Synthesis and characterization of ZIF-8 nanoparticles for controlled release of 6-mercaptopurine drug, *J. Drug Deliv. Sci. Technol.*, 2017, **41**, 106–112.

35 H. Wang, T. Li, J. Li, W. Tong and C. Gao, One-pot synthesis of poly(ethylene glycol) modified zeolitic imidazolate framework-8 nanoparticles: Size control, surface modification and drug encapsulation, *Colloids Surf., A*, 2019, **568**, 224–230.

36 F. Shu, D. Lv, X.-L. Song, B. Huang, C. Wang, Y. Yu and S.-C. Zhao, Fabrication of a hyaluronic acid conjugated metal–organic framework for targeted drug delivery and magnetic resonance imaging, *RSC Adv.*, 2018, **8**(12), 6581–6589.

37 C. Chu, H. Lin, H. Liu, X. Wang, J. Wang, P. Zhang, H. Gao, C. Huang, Y. Zeng, Y. Tan, G. Liu and X. Chen, Tumor Microenvironment-Triggered Supramolecular System as an In Situ Nanotheranostic Generator for Cancer Phototherapy, *Adv. Mater.*, 2017, **29**(23), 1605928.

38 D. Xu, Y. You, F. Zeng, Y. Wang, C. Liang, H. Feng and X. Ma, Disassembly of Hydrophobic Photosensitizer by Biodegradable Zeolitic Imidazolate Framework-8 for Photodynamic Cancer Therapy, *ACS Appl. Mater. Interfaces*, 2018, **10**(18), 15517–15523.

39 N. A. Soomro, Q. Wu, S. A. Amur, H. Liang, A. Ur Rahman, Q. Yuan and Y. Wei, Natural drug physcion encapsulated zeolitic imidazolate framework, and their application as antimicrobial agent, *Colloids Surf., B*, 2019, **182**, 110364.

40 Z. Xie, S. Liang, X. Cai, B. Ding, S. Huang, Z. Hou, P. a. Ma, Z. Cheng and J. Lin, O2-Cu/ZIF-8@Ce6/ZIF-8@F127 Composite as a Tumor Microenvironment-Responsive Nanoplatform with Enhanced Photo-/Chemodynamic Antitumor Efficacy, *ACS Appl. Mater. Interfaces*, 2019, **11**(35), 31671–31680.

41 Y. Zhao, Z. Song, X. Li, Q. Sun, N. Cheng, S. Lawes and X. Sun, Metal–organic frameworks for energy storage and conversion, *Energy Storage Materials*, 2016, **2**, 35–62.

42 W. Cai, C. C. Chu, G. Liu and Y. X. Wang, Metal-Organic Framework-Based Nanomedicine Platforms for Drug Delivery and Molecular Imaging, *Small*, 2015, **11**(37), 4806–4822.

43 L. Tang, J. Shi, X. Wang, S. Zhang, H. Wu, H. Sun and Z. Jiang, Coordination polymer nanocapsules prepared using metal–organic framework templates for pH-responsive drug delivery, *Nanotechnology*, 2017, **28**(27), 275601.

44 J. Zhuang, C.-H. Kuo, L.-Y. Chou, D.-Y. Liu, E. Weerapana and C.-K. Tsung, Optimized Metal–Organic-Framework Nanospheres for Drug Delivery: Evaluation of Small-Molecule Encapsulation, *ACS Nano*, 2014, **8**(3), 2812–2819.

45 Y. Wu, J. Wu, J. Cao, Y. Zhang, Z. Xu, X. Qin, W. Wang and Z. Yuan, Facile fabrication of poly(acrylic acid) coated chitosan nanoparticles with improved stability in biological environments, *Eur. J. Pharm. Biopharm.*, 2017, **112**, 148–154.

46 E. M. Wong, J. E. Bonevich and P. C. Searson, Growth Kinetics of Nanocrystalline ZnO Particles from Colloidal Suspensions, *J. Phys. Chem. B*, 1998, **102**(40), 7770–7775.

47 P. W. Voorhees, The theory of Ostwald ripening, *J. Stat. Phys.*, 1985, **38**(1), 231–252.

48 J. A. Thompson, K. W. Chapman, W. J. Koros, C. W. Jones and S. Nair, Sonication-induced Ostwald ripening of ZIF-8 nanoparticles and formation of ZIF-8/polymer composite membranes, *Microporous Mesoporous Mater.*, 2012, **158**, 292–299.

49 J. Cravillon, R. Nayuk, S. Springer, A. Feldhoff, K. Huber and M. Wiebcke, Controlling Zeolitic Imidazolate Framework Nano- and Microcrystal Formation: Insight into Crystal Growth by Time-Resolved In Situ Static Light Scattering, *Chem. Mater.*, 2011, **23**(8), 2130–2141.

50 S. V. Cleuvenbergen, Z. J. Smith, O. Deschaume, C. Bartic, S. Wachsmann-Hogiu, T. Verbiest and M. A. van der Veen, Morphology and structure of ZIF-8 during crystallisation measured by dynamic angle-resolved second harmonic scattering, *Nat. Commun.*, 2018, **9**, 3418.

51 J. Huang, R. Deng and K. Huang, Equilibria and kinetics of phenol adsorption on a toluene-modified hyper-cross-linked poly(styrene-co-divinylbenzene) resin, *Chem. Eng. J.*, 2011, **171**(3), 951–957.

52 C. Wu, D. Xie, Y. Mei, Z. Xiu, K. M. Poduska, D. Li, B. Xu and D. Sun, Unveiling the thermolysis natures of ZIF-8 and ZIF-67 by employing in situ structural characterization studies, *Phys. Chem. Chem. Phys.*, 2019, **21**(32), 17571–17577.

53 S. Wu, X. Zhao, Y. Li, Q. Du, J. Sun, Y. Wang, X. Wang, Y. Xia, Z. Wang and L. Xia, Adsorption Properties of Doxorubicin Hydrochloride onto Graphene Oxide: Equilibrium, Kinetic and Thermodynamic Studies, *Materials*, 2013, **6**(5), 2026–2042.

54 Y.-P. Wang, P. Zhou, S.-Z. Luo, X.-P. Liao, B. Wang, Q. Shao, X. Guo and Z. Guo, Controllable Synthesis of Monolayer Poly(acrylic acid) on the Channel Surface of Mesoporous Alumina for Pb(II) Adsorption, *Langmuir*, 2018, **34**(26), 7859–7868.

55 S. Anastasiou, N. Bhoria, J. Pokhrel and G. N. Karanikolos, *Metal Organic Framework Mixed Matrix Membranes for CO2 Separation*, Abu Dhabi International Petroleum Exhibition & Conference, Society of Petroleum Engineers, Abu Dhabi, UAE, 2016, p. 8.

56 Y. Si, Y. Li, J. Zou, X. Xiong, X. Zeng and J. Zhou, Photocatalytic Performance of a Novel MOF/BiFeO3; Composite, *Materials*, 2017, **10**(10), 1161.

57 N. Li, L. Zhou, X. Jin, G. Owens and Z. Chen, Simultaneous removal of tetracycline and oxytetracycline antibiotics from wastewater using a ZIF-8 metal–organic-framework, *J. Hazard. Mater.*, 2019, **366**, 563–572.

58 Y. Jiang, T. Li, M. Lu, D. Li, F. Ren, H. Zhao and Y. Li, TEMPO-oxidized starch nanoassemblies of negligible toxicity compared with polyacrylic acids for high performance anti-cancer therapy, *Int. J. Pharm.*, 2018, **547**(1), 520–529.

59 L. Huang, J. Wang, S. Huang, F. Siaw-Debrah, M. Nyanzu and Q. Zhuge, Polyacrylic acid-coated nanoparticles loaded with recombinant tissue plasminogen activator for the treatment of mice with ischemic stroke, *Biochem. Biophys. Res. Commun.*, 2019, **516**(2), 565–570.

60 I. Imaz, M. Rubio-Martínez, L. García-Fernández, F. García, D. Ruiz-Molina, J. Hernando, V. Puntes and D. Maspoch, Coordination polymer particles as potential drug delivery systems, *Chem. Commun.*, 2010, **46**(26), 4737–4739.

61 S. Scheiner, T. Kar and J. Pattanayak, Comparison of Various Types of Hydrogen Bonds Involving Aromatic Amino Acids, *J. Am. Chem. Soc.*, 2002, **124**(44), 13257–13264.

62 M. Hoop, C. F. Walde, R. Riccò, F. Mushtaq, A. Terzopoulou, X.-Z. Chen, A. J. deMello, C. J. Doonan, P. Falcaro, B. J. Nelson, J. Puigmartí-Luis and S. Pané, Biocompatibility characteristics of the metal–organic framework ZIF-8 for therapeutical applications, *Appl. Mater. Today*, 2018, **11**, 13–21.

63 S. H. Pang, C. Han, D. S. Sholl, C. W. Jones and R. P. Lively, Facet-Specific Stability of ZIF-8 in the Presence of Acid Gases Dissolved in Aqueous Solutions, *Chem. Mater.*, 2016, **28**(19), 6960–6967.

64 C.-Y. Sun, C. Qin, X.-L. Wang, G.-S. Yang, K.-Z. Shao, Y.-Q. Lan, Z.-M. Su, P. Huang, C.-G. Wang and E.-B. Wang, Zeolitic imidazolate framework-8 as efficient pH-sensitive drug delivery vehicle, *Dalton Trans.*, 2012, **41**(23), 6906–6909.

65 M. Laura Soriano, C. Carrillo-Carrion, C. Ruiz-Palomero and M. Valcárcel, Cyclodextrin-modified nanodiamond for the sensitive fluorometric determination of doxorubicin in urine based on its differential affinity towards β/γ-cyclodextrins, *Microchim. Acta*, 2018, **185**(2), 115.

66 Y. Lv, D. Ding, Y. Zhuang, Y. Feng, J. Shi, H. Zhang, T.-L. Zhou, H. Chen and R.-J. Xie, Chromium-Doped Zinc Gallogermanate@Zeolitic Imidazolate Framework-8: A Multifunctional Nanoplatform for Rechargeable In Vivo Persistent Luminescence Imaging and pH-Responsive Drug Release, *ACS Appl. Mater. Interfaces*, 2019, **11**(2), 1907–1916.

67 I. J. Macha, B. Ben-Nissan, E. N. Vilchevskaya, A. S. Morozova, B. E. Abali, W. H. Muller and W. Rickert, Drug Delivery From Polymer-Based Nanopharmaceuticals-An Experimental Study Complemented by Simulations of Selected Diffusion Processes, *Front. Bioeng. Biotechnol.*, 2019, **7**(37), 1–14.

68 H. Nabipour, M. H. Sadr and G. R. Bardajee, Synthesis and characterization of nanoscale zeolitic imidazolate frameworks with ciprofloxacin and their applications as antimicrobial agents, *New J. Chem.*, 2017, **41**(15), 7364–7370.

69 N. Ahmad, R. Ahmad, M. A. Alam and F. J. Ahmad, Enhancement of oral bioavailability of doxorubicin through surface modified biodegradable polymeric nanoparticles, *Chem. Cent. J.*, 2018, **12**(1), 65.

70 B. Tian, S. Liu, S. Wu, W. Lu, D. Wang, L. Jin, B. Hu, K. Li, Z. Wang and Z. Quan, pH-responsive poly (acrylic acid)-gated mesoporous silica and its application in oral colon targeted drug delivery for doxorubicin, *Colloids Surf., B*, 2017, **154**, 287–296.

71 R. Casasús, M. D. Marcos, R. Martínez-Máñez, J. V. Ros-Lis, J. Soto, L. A. Villaescusa, P. Amorós, D. Beltrán, C. Guillem and J. Latorre, Toward the Development of Ionically Controlled Nanoscopic Molecular Gates, *J. Am. Chem. Soc.*, 2004, **126**(28), 8612–8613.

72 M. Xu, J. Zhu, F. Wang, Y. Xiong, Y. Wu, Q. Wang, J. Weng, Z. Zhang, W. Chen and S. Liu, Improved In Vitro and In Vivo Biocompatibility of Graphene Oxide through Surface Modification: Poly(Acrylic Acid)-Functionalization is Superior to PEGylation, *ACS Nano*, 2016, **10**(3), 3267–3281.

73 L. L. Zheng, V. Vanchinathan, R. Dalal, J. Noolandi, D. J. Waters, L. Hartmann, J. R. Cochran, C. W. Frank, C. Q. Yu and C. N. Ta, Biocompatibility of poly(ethylene glycol) and poly(acrylic acid) interpenetrating network hydrogel by intrastromal implantation in rabbit cornea, *J. Biomed. Mater. Res., Part A*, 2015, **103**(10), 3157–3165.

74 L. R. de Moura Ferraz, A. É. G. A. Tabosa, D. D. S. da Silva Nascimento, A. S. Ferreira, V. de Albuquerque Wanderley Sales, J. Y. R. Silva, S. A. Júnior, L. A. Rolim, J. J. de Souza Pereira and P. J. Rolim-Neto, ZIF-8 as a promising drug delivery system for benznidazole: development, characterization, in vitro dialysis release and cytotoxicity, *Sci. Rep.*, 2020, **10**(1), 16815.

75 L. Latifi and S. Sohrabnezhad, Drug delivery by micro and meso metal–organic frameworks, *Polyhedron*, 2020, **180**, 114321.
76 H. Pham, K. Ramos, A. Sua, J. Acuna, K. Slowinska, T. Nguyen, A. Bui, M. D. R. Weber and F. Tian, Tuning Crystal Structures of Iron-Based Metal-Organic Frameworks for Drug Delivery Applications, *ACS Omega*, 2020, **5**(7), 3418–3427.
77 J. Bi, Y. Lu, Y. Dong and P. Gao, Synthesis of Folic Acid-Modified DOX@ZIF-8 Nanoparticles for Targeted Therapy of Liver Cancer, *J. Nanomater.*, 2018, **2018**, 1357812.
78 J. S. F. Silva, J. Y. R. Silva, G. F. de Sá, S. S. Araújo, M. A. G. Filho, C. M. Ronconi, T. C. Santos and S. A. Júnior, Multifunctional System Polyaniline-Decorated ZIF-8 Nanoparticles as a New Chemo-Photothermal Platform for Cancer Therapy, *ACS Omega*, 2018, **3**(9), 12147–12157.
79 M. Rezaei, A. Abbasi, R. Varshochian, R. Dinarvand and M. Jeddi-Tehrani, NanoMIL-100(Fe) containing docetaxel for breast cancer therapy, *Artif. Cells, Nanomed., Biotechnol.*, 2018, **46**(7), 1390–1401.
80 M. A. Simon, E. Anggraeni, F. E. Soetaredjo, S. P. Santoso, W. Irawaty, T. C. Thanh, S. B. Hartono, M. Yuliana and S. Ismadji, Hydrothermal Synthesize of HF-Free MIL-100(Fe) for Isoniazid-Drug Delivery, *Sci. Rep.*, 2019, **9**(1), 16907.